

# A Model Reference Adaptive Control-Based Speed Controller for a Surface-Mounted Permanent Magnet Synchronous Motor Drive

Anh Tuan Nguyen, Muhammad Saad Rifaq, Han Ho Choi, *Member, IEEE*, and Jin-Woo Jung, *Member, IEEE*

**Abstract**—This paper designs a simple model reference adaptive control-based speed controller (MRAC-SC) for a surface-mounted permanent magnet synchronous motor (SPMSM) drive. The proposed adaptive scheme is designed to track a reference model which ensures the desired exponential decay of controlled speed error trajectory. Also, the proposed MRAC method includes two control terms: an adaptive compensating control term and a stabilizing feedback control term. The former is proposed to compensate for uncertain model parameters (i.e., inertia, friction, and load torque) and the latter is constructed to asymptotically stabilize the error dynamics. The asymptotic stability of the closed-loop is guaranteed with both control terms using Lyapunov approach. The comparative studies between the proposed MRAC-SC, the non-adaptive model reference speed controller (NAMR-SC), and the conventional PI speed controller (PI-SC) are performed to justify a fast transient response, a good tracking possibility, and robustness against the parameter uncertainties of the proposed MRAC technique.

**Index Terms**—Cascade control structure, model reference adaptive control (MRAC), speed control, surface-mounted permanent magnet synchronous motor (SPMSM).

## I. INTRODUCTION

In recent years, the permanent magnet synchronous motors (PMSMs) have attracted great attention in industrial applications because of their advantages such as high efficiency, reliable operation, high power density, simple structure, and compact size [1]. For applications such as electric vehicles (EVs), elevators, ship electric propulsion systems, and industrial processes, the PMSM drives require a high control performance such as fast dynamic response and high-accuracy trajectory tracking [2]-[3]. To meet such requirements, numerous control methodologies have been employed such as cascade structure based on field-oriented control (FOC) and direct torque control (DTC).

Manuscript received September 15, 2017; revised December 22, 2017, February 21, 2018, and March 21, 2018; accepted March 24, 2018. This research was supported by Basic Science Research Program through the National Research Foundation of Korea (NRF) funded by the Ministry of Education (No. 2017R1D1A1B03030652).

The authors are with the Division of Electronics and Electrical Engineering, Dongguk University, Seoul 04620, Korea (e-mail: jinwjung@dongguk.edu).

Initially, the controllers of the PMSM drives use the traditional FOC based cascade structure with simple and separate control loops which accounts for most control structures in the industry [4]. Among the controllers with this popular structure, the proportional-integral (PI) controller, which is a long-standing linear control scheme, is also widely applied due to its relative simple implementation [5]-[7]. However, the PMSM drives are nonlinear time-varying systems with inevitable and immeasurable disturbances as well as parameter variations [8], [9]. These facts challenge the control design for a high-performance PMSM drive. Nowadays, thanks to the rapid progress of digital signal processors (DSPs), many nonlinear control methods such as sliding-mode control (SMC) [10]-[11], fuzzy control [12]-[13], and neural network control (NNC) [14]-[15] have been suggested for the PMSM drives. In [10], SMC demonstrates its robustness against model parameter uncertainties but the conventional chattering problem deteriorates the control performance. An improved SMC is presented in [11] to deal with the chattering problem. However, the robustness of the SMC is ensured for a bounded variation of specific parameters in the PMSM and its design heavily depends on the existence of a sliding surface. Fuzzy control methods employed in [12], [13] can deal with the nonlinearity of the PMSM by using simple inference rules. However, this method involves the human experience with membership functions and inference rules presented in an unsystematic approach [13]. Such important questions on how to ensure the system stability and how to generalize the fuzzy control design into other applications are still opened. NNC is one of artificial intelligence based methods introduced in [14]-[15] with the advantage of the online learning abilities. Both [14]-[15] show a high potential for NNC to deal with the nonlinear relationship and unmodeled parts in the PMSM model. However, there are numerous issues to achieve a clear solution in a real application such as the selection of a neural network structure, the online computational burden, the way of training the network, and the stability problem of the overall control system.

In variable-speed motor drives, adaptive control is one of the most effective methods that can solve the parametric uncertainties and disturbances with online adaptive rules. In [16]-[20], several adaptive controllers are presented in different design targets such as adaptive gains PID control [16], adaptive fuzzy control [17]-[18], adaptive compensating

feedback control [19]-[20]. Among the adaptive control methods, the model reference adaptive control (MRAC) offers a systematic design approach by a well-defined reference model that the system follows [21]. The MRAC can regulate the parameters of a controller under the parameter variations by comparing the system output response with a stabilized reference model to stabilize the overall dynamics of a feedback control system [22]. A number of efforts are being made to improve the robustness against the parameter variations by using MRAC scheme for the diverse plants such as in [23]-[26]. In [23], the instantaneous and steady-state values are used in the reference model of the MRAC configuration to estimate the rotor speed in the sensorless control for an induction motor drive. Meanwhile, a disturbance estimator is combined with MRAC [24] to compensate for the parameter variations in the current regulator while the shortcomings of the employed PI speed controller remain unattended. Guo and Parsa [25] propose a MRAC scheme for the five-phase interior PMSM but did not provide the details on the stability analysis. In [26], a second-order term is selected as a reference model with an additional online tuning controller which requires extensive computations for better transient and steady state tracking performance. Henceforth, in spite of the effectiveness of the MRAC method in anti-uncertainties of parameters for ac motor drives, the high-order terms in the reference model increase the computational burden and the overall stability is often left unproven.

This paper proposes a simple MRAC-based speed controller (MRAC-SC) for a surface-mounted permanent magnet synchronous motor (SPMSM) drive. The proposed scheme can guarantee the fast exponential decay of the speed error trajectory following a given reference model regardless of uncertain parameters and load disturbances. In addition, the proposed control law is designed with two control terms: an adaptive compensating control term and a stabilizing feedback control term. First, the adaptive control term compensates for the uncertainties and disturbances, whereas the stabilizing control term asymptotically stabilizes the error dynamics. A Lyapunov function is used to develop the adaptive control law and then the asymptotic stability of the closed-loop is justified with both control terms. In this paper, the non-adaptive model reference speed controller (NAMR-SC) and the conventional PI speed controller (PI-SC) are selected to compare the performance of the proposed MRAC scheme. The comparative results using both a MATLAB/Simulink package and a prototype SPMSM drive test-bench controlled by a TI TMS320F28335 DSP verify the superiority (e.g., a fast transient response, a good tracking possibility, and robustness against uncertain parameters and load disturbances) of the proposed MRAC method under various operating scenarios.

This paper is constructed into six sections including the first introduction section. In Section II, the dynamic model of the SPMSM is developed in a synchronous  $d$ - $q$  rotating frame for the overall control design and the popular PI current controllers in an inner loop of a cascade control structure are

briefly reviewed. Section III presents the NAMR-SC and then proposes the MRAC-SC. Section IV presents the comparative studies and results from both simulations and experiments to verify the performances of the proposed method. Finally, Section V draws a conclusion for the work of this paper.

## II. DYNAMIC MODEL AND PI CURRENT CONTROLLER FOR SPMSM DRIVES

### A. Surface-Mounted PMSM Model

The mechanical and electrical dynamic equations of a surface-mounted PMSM in the synchronous  $d$ - $q$  rotating frame [3] are given as

$$\begin{cases} \dot{\omega} = g_1 i_{qs} - g_2 \omega - g_3 T_L \\ \dot{i}_{qs} = -g_4 i_{qs} - g_5 \omega + g_6 u_{qs} - \omega i_{ds} \\ \dot{i}_{ds} = -g_4 i_{ds} + g_6 u_{ds} + \omega i_{qs} \end{cases} \quad (1)$$

where

$$\begin{aligned} g_1 &= \frac{3}{2} \frac{1}{J} \frac{p^2}{4} \varphi_f, & g_2 &= \frac{B}{J}, & g_3 &= \frac{p}{2J}, \\ g_4 &= \frac{R_S}{L_S}, & g_5 &= \frac{\varphi_f}{L_S}, & g_6 &= \frac{1}{L_S}. \end{aligned} \quad (2)$$

$i_{qs}$  and  $i_{ds}$  are the  $q$ -axis and  $d$ -axis stator currents,  $u_{qs}$  and  $u_{ds}$  are the  $q$ -axis and  $d$ -axis stator voltages (control inputs),  $\omega$  is the electrical rotor speed (controlled output),  $R_S$  is the stator resistance,  $L_S$  is the stator inductance,  $T_L$  is the load torque,  $J$  is the rotor moment of inertia,  $B$  is the viscous friction coefficient,  $p$  is the number of poles, and  $\varphi_f$  is the magnet flux linkage.

Let  $i_{ds}$ ,  $i_{qs}$ , and  $\omega$  be defined as the state variables for state-space based control design. In the proposed adaptive control design, the parameters in (2) (i.e.,  $g_1, g_2, \dots, g_6$ ) are considered to be unknown and vary slowly during a short sampling time, so they can be set as  $\dot{g}_i = 0$ . Additionally, the load torque is unknown and slowly varies in a short sampling period, hence, it can be set as  $\dot{T}_L = 0$ .

### B. PI Current Controllers in an Inner Loop of Cascade Control Structure

Fig. 1 presents the cascade control system in order to efficiently control the three state variables (i.e.,  $i_{ds}$ ,  $i_{qs}$ , and  $\omega$ ) of SPMSMs such that the inner-loop regulates the two  $dq$ -axis currents ( $i_{qs}$ ,  $i_{ds}$ ), whereas the outer-loop regulates the rotor speed ( $\omega$ ) to the desired set points. In order to prevent possible inner disturbances from propagating to the outer loop, the bandwidth of the inner current loop is chosen with at least five times higher value than that of the outer speed loop [27]. In particular, the PI current controller is extensively utilized in the inner loop to fast and properly regulate the stator currents in the final target of reducing the current ripples in the motor drive systems. For this reason, the control voltage commands in the synchronous  $d$ - $q$  rotating frame (i.e.,  $u_{qs}$  and  $u_{ds}$ ) for the SPMSM drive are generated by the PI current controllers as follows:

$$u_{qs} = K_P (i_{qsd} - i_{qs}) + K_I \int_0^t (i_{qsd} - i_{qs}) d\tau \quad (3)$$

$$u_{ds} = K_P (i_{dsd} - i_{ds}) + K_I \int_0^t (i_{dsd} - i_{ds}) d\tau$$

where  $K_P$  and  $K_I$  are the control gains. The  $d$ -axis current reference ( $i_{dsd}$ ) is set as zero owing to the rotor non-saliency whereas the  $q$ -axis current reference ( $i_{qsd}$ ) is set by the speed control loop, which can reduce the torque ripples [5]. Although the PI controller can be employed for the speed control loop, it is not easy to attain the good tracking performance with zero steady-state error under the disturbances and parameter variations.

Finally, to overcome the above mentioned shortcomings of the PI speed controller (PI-SC), this paper proposes a robust speed controller based on the MRAC which compensates for steady-state error as well as nonlinearity terms under parameter uncertainties. The next section will describe in detail the MRAC-based speed controller (MRAC-SC) design and its stability analysis.

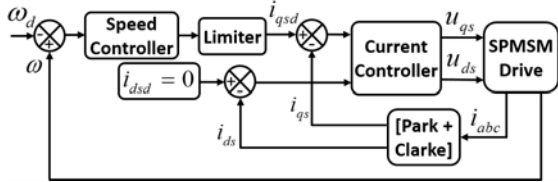


Fig. 1. Typical architecture of a general SPMSM drive using a cascade control structure.

### III. PROPOSED MRAC-BASED SPEED CONTROLLER DESIGN AND STABILITY ANALYSIS

This section first presents the non-adaptive model reference speed controller (NAMR-SC) and then proposes the MRAC-SC and its stability analysis. Note that the NAMR-SC is an intermediate controller to design the proposed MRAC-SC. First, a reference model is introduced, which produces an exponential damping curve for the speed error to follow. Then the proposed MRAC-based speed control law is designed to incorporate two control terms: a stabilizing feedback term and an adaptive compensating term. Finally, a systematic design to implement the proposed control law is described in detail.

#### A. Reference Model for Speed Controller Design

The MRAC assures the dynamic performance of the feedback system by properly choosing the reference model [22]. In the traditional MRAC forms [25], the reference model electrical rotor speed ( $\omega_m$ ) is compared directly to the feedback speed ( $\omega$ ). However, in this paper, the reference model output is compared to the electrical speed error ( $\omega_e = \omega - \omega_d$ ) between the actual speed ( $\omega$ ) and the desired speed ( $\omega_d$ ), which guarantees the good tracking performance of the proposed MRAC-SC. From (1), the reference model can be chosen as the following first-order differential equation:

$$\dot{\omega}_m + \lambda_m \omega_m = 0 \quad (4)$$

where  $\lambda_m$  is a strictly positive constant parameter, and  $\omega_m$  is the output of the reference model that has the exponential decay form as

$$\omega_m = c e^{-\lambda_m t} \quad (5)$$

where  $c > 0$  is derived from the initial condition. Since the first equation in (1) is the first-order derivative of the speed, the reference model (4) is also the first-order derivative of the output of the reference model that has the solution (5) with an exponential decay function.

By using the error vector  $e = [e_1, e_2]^T$ , the following error dynamic model can be obtained:

$$\begin{aligned} \dot{e}_1 &= e_2 \\ \dot{e}_2 &= g_1 i_{qsd} - g_2 \omega - g_3 T_L + \lambda_m \omega_m \end{aligned} \quad (6)$$

where  $e_2 = e_\omega = \omega_e - \omega_m$  and  $e_1 = \int_0^t e_\omega d\tau = \int_0^t e_2 d\tau$ . It is noted that the desired speed ( $\omega_d$ ) varies slowly for a short sampling period, so  $\dot{\omega}_d = \ddot{\omega}_d = 0$ .

Let a combined tracking error  $\sigma$  be defined by

$$\sigma = \gamma e_1 + e_2 \quad (7)$$

where  $\gamma$  is an arbitrary positive constant.

The following lemma is used to form the important link of a controller design.

*Lemma 1:* There exists a constant parameter vector  $\psi^* = [\psi_1^*, \psi_2^*, \psi_3^*]^T$  such that

$$g_1 h^T \psi^* = g_1 \sum_{i=1}^3 h_i \psi_i^* = g_2 \omega - \gamma \omega + \gamma \omega_m - \lambda_m \omega_m - \gamma \omega_d - g_3 T_L \quad (8)$$

where  $h = [h_1, h_2, h_3]^T = [\omega, \omega_m, 1]^T$ .

*Proof:* As mentioned in the above assumption, the load torque and parameters are unknown and set as  $\dot{T}_L = 0$  and  $\dot{g}_i = 0$ . Therefore, all the parameters  $\gamma$ ,  $\lambda_m$ ,  $\omega_d$ ,  $g_2$ , and  $T_L$  can be assumed to be constant. This implies that (8) holds with

$$\psi^* = -\frac{1}{g_1} [\gamma - g_2, \lambda_m - \gamma, \gamma \omega_d + g_3 T_L]^T \quad (9)$$

Also, from this assumption, its time derivative is equal to zero ( $\dot{\psi}^* = 0$ ).

The next subsection will introduce the non-adaptive model reference control law in order to compare the proposed adaptive model reference control law.

#### B. Non-Adaptive Model Reference Speed Controller Design

*Theorem 1:* If the parameters of SPMSMs are known, to achieve a perfect tracking control, let the reference  $q$ -axis current  $i_{qsd}$  be given by a stabilizing feedback control term ( $-\kappa \sigma$ ) and a non-adaptive compensating control term ( $\psi^{*T} h$ ) below:

$$i_{qsd} = -\kappa \sigma + \psi^{*T} h \quad (10)$$

where  $\kappa > 0$ . Then,  $e$  converges to zero.

*Proof:* The Lyapunov function is defined as follows:

$$V = \frac{\sigma^2}{2} \quad (11)$$

Then, the time derivative of  $V(t)$  is obtained as

$$\dot{V}(t) = \sigma \dot{\sigma} \quad (12)$$

On the other hand, (6) implies that

$$\dot{\sigma} = \gamma \dot{e}_1 + \dot{e}_2 = \gamma e_2 + g_1 i_{qsd} - g_2 \omega - g_3 T_L + \lambda_m \omega_m. \quad (13)$$

Therefore, (12) can be expanded as

$$\begin{aligned} \dot{V} &= \sigma(\gamma e_2 + g_1 i_{qsd} - g_2 \omega - g_3 T_L + \lambda_m \omega_m) \\ &= \sigma \left[ g_1 i_{qsd} + (\gamma - g_2) \omega + (\lambda_m - \gamma) \omega_m - \gamma \omega_d - g_3 T_L \right]. \end{aligned} \quad (14)$$

Lemma 1 and (14) imply that

$$\dot{V} = -g_1 \kappa \sigma^2 \leq 0 \quad (15)$$

which shows that  $e$  converges to zero.

From (10), this law implies that

$$i_{qsd} = -\kappa \sigma - \frac{(\gamma - g_2) \omega - (\lambda_m - \gamma) \omega_m - \gamma \omega_d - g_3 T_L}{g_1}. \quad (16)$$

Note that the first term in (16), i.e., the stabilizing feedback term, is specially designed based on a model reference technique by employing the speed error ( $e_2 = e_\omega = \omega_e - \omega_m$ ) as the difference between the feedback speed error ( $\omega_e$ ) and the reference model speed ( $\omega_m$ ). This special approach allows a flexible choice of the whole reference dynamics to accurately track the desired rotor speed. However, the conventional PI controller directly uses the difference between the measured speed ( $\omega$ ) and the desired speed ( $\omega_d$ ) to create the feedback error. Next, the second term in (16) can improve the dynamic performance being faster and more robust than the conventional PI-SC because of employing the reference model. Fig. 2(a) and (b) show the block diagrams in order to clearly highlight the difference between the NAMR-SC and the conventional PI-SC for a SPMSM drive.

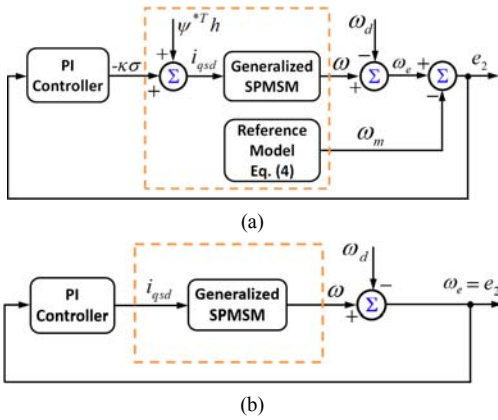


Fig. 2. Block diagrams of the two control schemes for a SPMSM drive. (a) The NAMR-SC. (b) The conventional PI-SC.

### C. Model Reference Adaptive Control (MRAC)-based Speed Controller Design and Stability Analysis

The proposed MRAC-SC includes two control terms: a stabilizing feedback control term and an adaptive compensating control term. The former is employed to asymptotically stabilize the error dynamics. Meanwhile, the latter is proposed to compensate for uncertainty parameters. Theorem 2 below proves the asymptotic stability of the closed-loop by using Lyapunov approach.

**Theorem 2:** If the parameters of SPMSMs are unknown, let the reference  $q$ -axis current  $i_{qsd}$  be given by a stabilizing feedback control term ( $-\kappa\sigma$ ) and an adaptive compensating

control term ( $\hat{\psi}^T h$ ) below:

$$i_{qsd} = -\kappa \sigma + \hat{\psi}^T h \quad (17)$$

where  $\hat{\psi}$  is an estimate of  $\psi^*$  given by the following update law:

$$\dot{\hat{\psi}} = -\Phi^{-1} h \sigma \quad (18)$$

where  $\Phi = \text{diag}(\varphi_1, \varphi_2, \varphi_3) > 0$  is the adaptation gain. Then,  $e$  converges to zero and  $\hat{\psi}$  is bounded.

*Proof:* The definition of Lyapunov function is written as follows:

$$V = \frac{(\sigma^2 + g_1 \tilde{\psi}^T \Phi \tilde{\psi})}{2} \quad (19)$$

where  $\tilde{\psi} = \psi^* - \hat{\psi}$ .

Then, the derivative of  $V(t)$  over time is given as

$$\begin{aligned} \frac{dV}{dt} &= \frac{1}{2} \left( 2\sigma \frac{d\sigma}{dt} + 2g_1 \tilde{\psi}^T \Phi \frac{d\tilde{\psi}}{dt} \right) \\ &= \sigma \dot{\sigma} + g_1 \tilde{\psi}^T \Phi (\dot{\psi}^* - \dot{\hat{\psi}}) \\ &= \sigma(\gamma \dot{e}_1 + \dot{e}_2) + g_1 \tilde{\psi}^T h \sigma \end{aligned} \quad (20)$$

Lemma 1 and (20) imply that

$$\begin{aligned} \dot{V} &= \sigma(g_1 i_{qsd} - g_1 \psi^{*T} h) + g_1 \psi^{*T} h \sigma - g_1 \hat{\psi}^T h \\ &= \sigma(-g_1 \kappa \sigma + g_1 \hat{\psi}^T h - g_1 \psi^{*T} h) + g_1 \psi^{*T} h \sigma - g_1 \hat{\psi}^T h \\ &= -g_1 \kappa \sigma^2 \leq 0 \end{aligned} \quad (21)$$

Integrating both sides of (21) gives

$$\int_0^\infty \dot{V}(\tau) d\tau = -g_1 \kappa \int_0^\infty \sigma^2 d\tau$$

or equivalently

$$V(\infty) - V(0) \leq -g_1 \kappa \int_0^\infty \sigma^2 d\tau. \quad (22)$$

Thus, the above inequality can be rewritten as

$$g_1 \kappa \int_0^\infty \sigma^2 d\tau \leq V(0) - V(\infty) \leq V(0) \quad (23)$$

when using  $V(t) \geq 0$ . Then, the following inequality can be derived

$$\int_0^\infty \sigma^2 d\tau \leq \infty \quad (24)$$

which implies that  $\sigma \in L_2$ . Since  $\dot{V} \leq 0$  as shown in (23),  $V(t)$  is nonincreasing and has an upper bound (i.e.,  $V(t) \leq V(0)$ ). This implies that  $\sigma \in L_\infty$ ,  $\hat{\psi} \in L_\infty$ .

From the tracking error (7), the transfer function  $G(s)$  from  $\sigma$  to  $e_1$  is expressed by the following strictly positive real function:

$$G(s) = \frac{1}{s + \gamma}. \quad (25)$$

Finally, thanks to the result of [28], it can conclude that the error  $e_1$  converges to zero.

The above update law (18) implies that

$$\hat{\psi} = \begin{bmatrix} \hat{\psi}_1 \\ \hat{\psi}_2 \\ \hat{\psi}_3 \end{bmatrix} = - \begin{bmatrix} \int_0^t \frac{\sigma \omega}{\varphi_1} d\tau & \int_0^t \frac{\sigma \omega_m}{\varphi_2} d\tau & \int_0^t \frac{\sigma}{\varphi_3} d\tau \end{bmatrix}^T. \quad (26)$$

From (26), the second term of (17) can be derived as follows:

$$\hat{\psi}^T h = - \left( \omega \int_0^t \frac{\sigma \omega}{\varphi_1} d\tau + \omega_m \int_0^t \frac{\sigma \omega_m}{\varphi_2} d\tau + \int_0^t \frac{\sigma}{\varphi_3} d\tau \right). \quad (27)$$

Note that, the first term in (17) is similar to that of the NAMR-SC. Meanwhile, (27) represents in detail the adaptive compensating control term (i.e., the second term in (17)) of the proposed adaptive control law (17). Thus, the proposed scheme yields a robust capability against the external disturbances and the parameter variations due to the absence of both load torque and parameters. Fig. 3 illustrates the complete block diagram of the proposed MRAC-SC for a SPMSM drive.

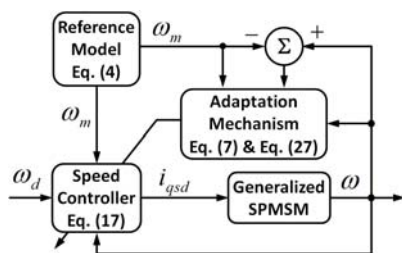


Fig. 3. Block diagram of the proposed MRAC-SC for a SPMSM drive.

*Remark 1:* First, the stability of the proposed MRAC-SC is ensured by the first term in (17) which depends on the coefficient gains  $\kappa$  and  $\gamma$ . These gains are calculated based on the bandwidth of the speed controller [27]. Second, the robustness of the proposed MRAC-SC is guaranteed by the second term in (17) which is considered as the online tuning term due to the independence of this term on the parameter variations. Thus, the adaptation gain matrix  $\Phi = \text{diag}(\varphi_1, \varphi_2, \varphi_3)$  is selected based on the tradeoff between the fast transient response and small steady-state tracking error [25]. Moreover, the  $\Phi$  should be a positive large value to be robust against the external disturbances and parameter variations of the proposed MRAC-SC.

#### D. Systematic Design Procedure to Implement a Robust MRAC-Based Speed Controller

Here, a robust MRAC-SC can be completely designed based on the below design procedure:

- Step 1)** Build the system model (1) in the synchronously rotating  $d$ - $q$  reference frame.
- Step 2)** Choose the design parameter  $\lambda_m$  with a large value and the initial value  $c$  with a small value for the reference model (5) to meet the fast response requirement.
- Step 3)** Set the gains of the PI decoupling current controller in (3) based on the general tuning rules [24], [27]. It should be chosen with the high values to achieve the fast response performance of the controller.
- Step 4)** Set the adaptation gain matrix  $\Phi$  in (18) with the large values because this gain determines the convergence of the response when suddenly introducing the desired speed. Thus the adaptation gain is tuned by a specified amount to achieve the good performance.

**Step 5)** Choose the coefficient  $\kappa$  for (10) as well as (17). Actually, the first term in (10) or (17) can be regarded as a PI controller. Thus, it should be tuned increasingly to reduce the overshoot in case of a sudden change. If the acceptable transient performance is obtained, then quit, or else, return to *Step 3*.

## IV. CASE STUDY FOR VERIFICATIONS

### A. Test-Bench Description

To evaluate the performance of the proposed MRAC-SC for the SPMSM drive, a computer simulation model with MATLAB/Simulink and experiments on a prototype SPMSM drive were carried out with the nominal parameters in Table I.

Fig. 4 depicts a prototype SPMSM drive system with a Texas Instruments (TI) TMS320F28335 DSP. This experimental setup includes five parts: a SPMSM, a three-phase pulse-width modulation (PWM) inverter, an electrical brake, an incremental encoder, and a control board with a TI TMS320F28335 DSP. As depicted in Fig. 4, the dc-link voltage ( $V_{dc}$ ) is provided from the alternating current (ac) mains voltage (AC 220 V/60 Hz) via a single-phase H-bridge rectifier. Then, the three-phase PWM inverter transfers the electric power from the dc-link to a three-phase SPMSM. The two phase currents ( $i_a, i_b$ ) flowing in the stator windings are fed to the input ports of a 12-bit analog-to-digital converters (ADC) via two Hall-effect current sensors. Also, the motor speed is calculated from the position ( $\theta$ ) obtained by an optical incremental encoder E40HB-2500 mounted coaxially with the motor. Finally, a space-vector PWM (SVPWM) technique is chosen as an effective PWM method which is reported with less harmonics distortion than other PWM methods [29].

In the simulation and experimental studies, the SPMSM drive is run with a sampling time ( $T_s$ ) of 200  $\mu$ s and a PWM switching frequency of 5 kHz. It is noted that the selected bandwidth (i.e., 180 Hz or 1130 rad/s) of the PI current controller should be 20 times smaller than that of the switching frequency [27]. To design the reference model (4),  $\lambda_m$  should be a positive number which is chosen with the value of 1000, and the parameter  $c$  in (5) derived from the initial condition is set as a value of 0.25 to guarantee that the slope of the model reference ( $\omega_m$ ) approaches zero. It should be noted that when the reference speed is negative, the parameter  $c$  can be negative and the initial value of the speed error can be positive (i.e.,  $|\omega_d| > |\omega|$ ). Thus, the proposed MRAC-SC still uses the error between the speed error ( $\omega_e$ ) and the model reference speed ( $\omega_m$ ) as the feedback signal. Based on *Remark 1*, the gains ( $\kappa, \gamma$ ) for the stabilizing feedback control term in (10) and (17) are chosen as  $\kappa = 0.17$  and  $\gamma = 188$ . The gains for the non-adaptive compensating control term in (9) are simply calculated as  $\psi^* = [-0.1662, -0.716, -54.44]$ , whereas the gains for the adaptive compensating control term in (17) are set as  $\Phi = \text{diag}(10000, 10000, 10000)$  by following the *Remark 1*.

As described in Fig. 4, all blocks in the dotted line are

carried out by the DSP. To reveal the control performance of the proposed MRAC-SC and the NAMR-SC, the step tracking response (i.e. step change of speed and load torque) and the sinusoidal tracking response are investigated. Also, the conventional PI-SC is employed to evaluate the tracking performance of the proposed MRAC-SC. Thus, the above three control schemes are implemented under the following three cases as illustrated in Table II: *Case 1*: a step speed change (i.e., 750 r/min  $\rightarrow$  1500 r/min) under the load torque ( $T_L$ ) set at 1.2 N·m, *Case 2*: a step load torque change (i.e., 1.2 N·m  $\rightarrow$  2.4 N·m) under the speed command set at 750 r/min, *Case 3*: a sinusoidal speed change with an amplitude of  $\pm 100$  r/min and a frequency of 5 Hz (i.e.,  $750 + 100\sin(10\pi \cdot t)$  r/min) under the load torque ( $T_L$ ) set at 1.2 N·m. In addition, to evaluate the robustness of the proposed MRAC-SC, all three cases are conducted with the parameter variations (i.e., +50% variations of  $J$ , +100% variations of  $B$ , -25% variations of  $\varphi_f$ , and +20% variations of  $L_S$ ). First, *Case 1* is selected to evaluate the transient performance when the desired rotor speed ( $\omega_d$ ) suddenly changes from the low speed to the medium speed at a constant load torque. Second, *Case 2* is chosen to verify the fast recovery possibility of the proposed MRAC-SC when having the abrupt change of load torque from half to the rated value. Finally, *Case 3* is selected to verify the sinusoidal tracking capability that may be needed for some industrial applications such as industrial robots in manufacturing industry.

TABLE I  
WORKSHOP SPMSM PARAMETERS

Rated power	750 [W]
Rated current	4.3 [A]
Rated load torque	2.4 [N·m]
Stator resistance $R_S$	0.43 [ $\Omega$ ]
Number of poles $p$	8
Stator inductance $L_S$	$3.2 \times 10^{-3}$ [H]
Magnet flux linkage $\varphi_f$	0.085 [V·s/rad]
Viscous friction coefficient $B$	$0.2 \times 10^{-3}$ [N·m·s/rad]
Equivalent rotor inertia $J$	$1.8 \times 10^{-3}$ [kg·m <sup>2</sup> ]

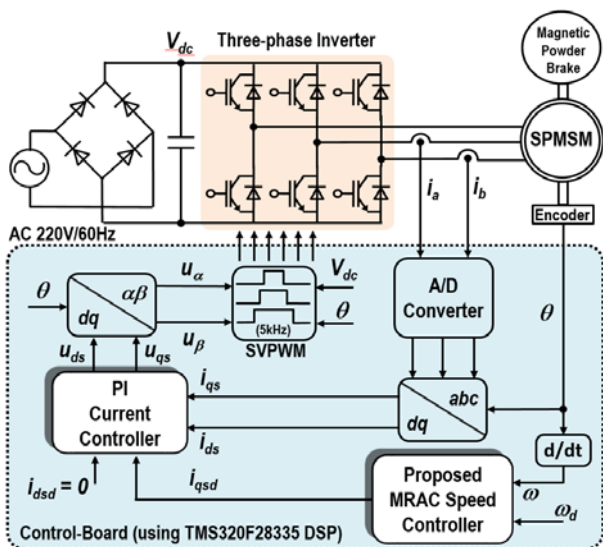


Fig. 4. Experimental setup of a prototype SPMSM drive system.

Also, in order to quantitatively evaluate the fast dynamic response of the controlled system, the controller bandwidth is used as one of the widely used criteria in control system design, so the sinusoidal speed reference tracking capability is a practical method to directly examine the bandwidth of the speed controller. In this case, to reduce the phase lag between the reference speed and the actual speed, and to keep the steady-state tracking error being small, the frequency of the sinusoidal speed reference is usually chosen between 10% and 50% of the speed loop bandwidth [30], [31]. Thus, the frequency of the sinusoidal speed command under this case is chosen as 5 Hz (= about 20% of the speed loop bandwidth (i.e., 25 Hz), which is set as 7 times smaller value than the bandwidth (i.e., 180 Hz) of the PI current controller [32], [33]).

TABLE II  
THREE CASE STUDIES FOR SIMULATION AND EXPERIMENT

Cases	Descriptions	Details	Parameter Uncertainties
1	Speed step response	$\omega_d$ : 750 r/min $\rightarrow$ 1500 r/min; $T_L$ : 1.2 N·m	+50% variations of $J$ , +100% variations of $B$ ,
2	Load torque step response	$\omega_d$ : 750 r/min; $T_L$ : 1.2 N·m $\rightarrow$ 2.4 N·m $\rightarrow$ 1.2 N·m	-25% variations of $B$ ,
3	Sinusoidal speed tracking response	$\omega_d$ : $750 + 100\sin(10\pi \cdot t)$ r/min; $T_L$ : 1.2 N·m	+20% variations of $L_S$

### B. Comparative Simulation Results between Proposed MRAC-SC, NAMR-SC, and Conventional PI-SC

Fig. 5(a)-(c) illustrate the comparative simulation results of the MRAC-SC, the NAMR-SC, and the conventional PI-SC for a step speed change (i.e., *Case 1*) under parameter variations, respectively. It is observed from Fig. 5(a) that the proposed MRAC-SC has a fast speed response with a short settling time (39 ms) and no overshoot. Fig. 5(b) shows that the NAMR-SC has a slower speed response with the settling time of 51 ms and no overshoot. Meanwhile, Fig. 5(c) depicts that the conventional PI-SC has the slowest speed response with the settling time of 63 ms. Hence, in this case, the proposed scheme consistently outperforms the NAMR-SC and the conventional PI-SC.

Fig. 6(a)-(c) present the comparative simulation results of the proposed MRAC-SC, the NAMR-SC, and the conventional PI-SC for a load step change from 1.2 N·m to 2.4 N·m and vice versa (i.e., *Case 2*) under parameter variations, respectively. Fig. 6(a) shows a more stable speed response (settling time: 29 ms) and a small overshoot (0.06%), whereas Fig. 6(b) shows much poorer speed response (i.e., settling time: 51 ms and speed overshoot: 0.16%) during the transient-state when the load torque abruptly changes. In Fig. 6(c), the speed response of the conventional PI-SC shows the settling time of 73 ms and speed overshoot of 0.25%. It is observed from Fig. 6 that the speed transient responses for the proposed MRAC-SC are quickly recovered due to its capability in suppressing the abrupt external disturbances.

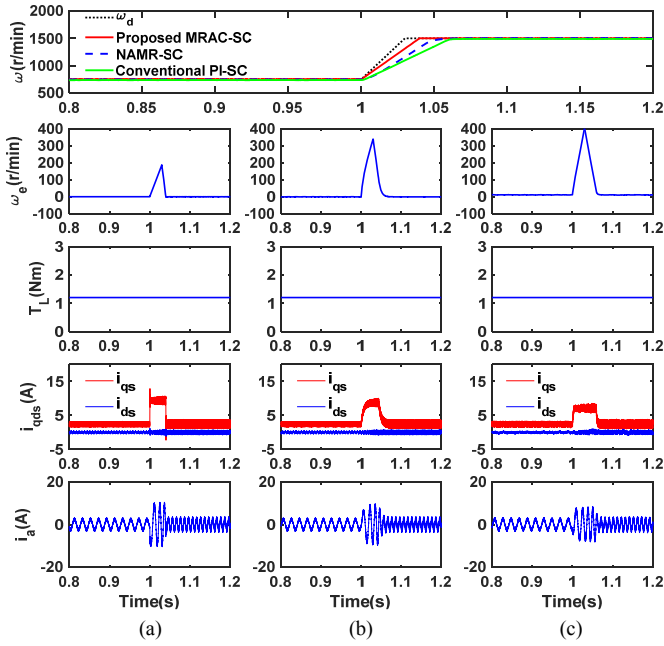


Fig. 5. Simulation results for Case 1 under parameter variations (i.e., +50% variations of  $J$ , +100% variations of  $B$ , -25% variations of  $\varphi_r$  and +20% variations of  $L_s$ ). (a) The proposed MRAC-SC. (b) The NAMR-SC. (c) The conventional PI-SC.

Fig. 7(a)-(c) show the comparative simulation results of the proposed MRAC-SC, the NAMR-SC, and the conventional PI-SC for a sinusoidal speed reference of  $750 + 100\sin(10\pi t)$  r/min (i.e., Case 3) under nominal parameters, respectively. Fig. 7(a) exhibits that the maximum speed error of the proposed MRAC-SC (7.5 r/min) is much smaller than those of the NAMR-SC (16 r/min) in Fig. 7(b) and the conventional PI-SC (22 r/min) in Fig. 7(c).

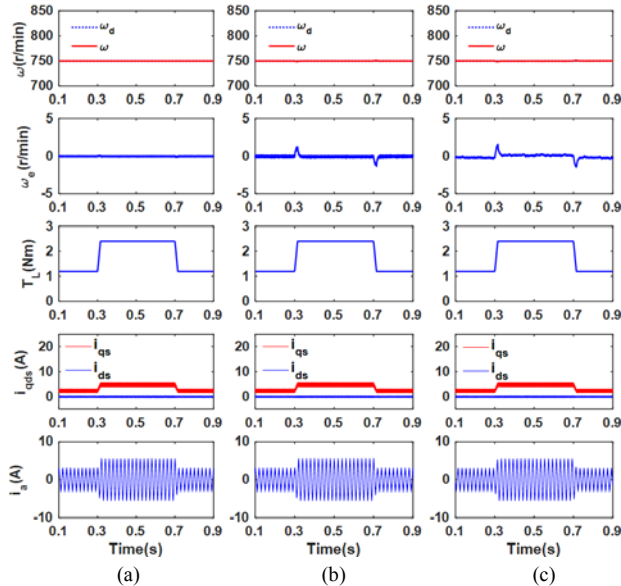


Fig. 6. Simulation results for Case 2 under parameter variations (i.e., +50% variations of  $J$ , +100% variations of  $B$ , -25% variations of  $\varphi_r$  and +20% variations of  $L_s$ ). (a) The proposed MRAC-SC. (b) The NAMR-SC. (c) The conventional PI-SC.

Fig. 8(a)-(c) show the comparative simulation results of

the proposed MRAC-SC, the NAMR-SC, and the conventional PI-SC for a sinusoidal speed reference of  $750 + 100\sin(10\pi t)$  r/min (i.e., Case 3) under parameter variations, respectively. Fig. 8(a) exhibits that the maximum speed error of the proposed MRAC-SC (8 r/min) is much smaller than those of the NAMR-SC (17 r/min) in Fig. 8(b) and the conventional PI-SC (26 r/min) in Fig. 8(c). From Figs. 7 and 8, this observation reveals that the sinusoidal speed tracking performance of the proposed MRAC-SC is much better compared to the NAMR-SC and the conventional PI-SC. Table III summarizes the performance comparisons of three control schemes during the transient-time through the simulation results.

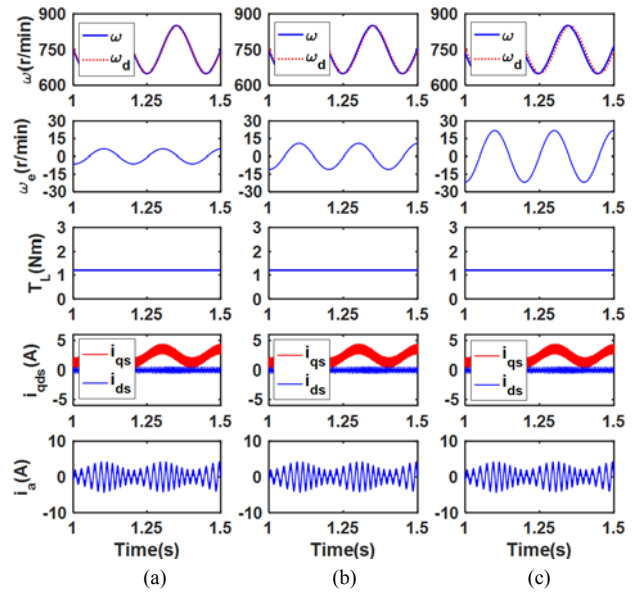


Fig. 7. Simulation results for Case 3 under nominal parameters. (a) The proposed MRAC-SC. (b) The NAMR-SC. (c) The conventional PI-SC.

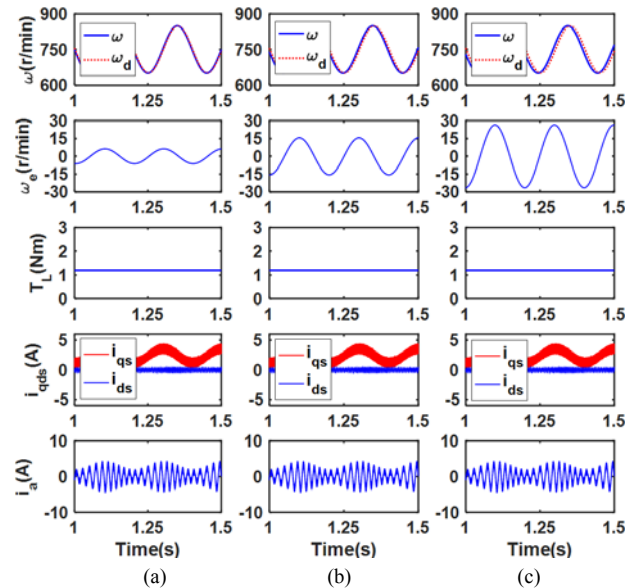


Fig. 8. Simulation results for Case 3 under parameter variations (i.e., +50% variations of  $J$ , +100% variations of  $B$ , -25% variations of  $\varphi_r$  and +20% variations of  $L_s$ ). (a) The proposed MRAC-SC. (b) The NAMR-SC. (c) The conventional PI-SC.

TABLE III

CONTROL PERFORMANCE COMPARISONS OF THREE CONTROL SCHEMES DURING THE TRANSIENT TIME VIA SIMULATION RESULTS

(i) / (ii) / (iii)		Case 1 under parameter variations	Case 2 under parameter variations	Case 3 under nominal parameter	Case 3 under parameter variations
Maximum Speed Error (r/min)	(i)	187.4	0.5	7.5	8
	(ii)	338.5	1.2	16	17
	(iii)	398.5	1.9	22	26
Overshoot (%)	(i)	0	0.06	-	-
	(ii)	0	0.16	-	-
	(iii)	0	0.25	-	-
Settling Time (ms)	(i)	39	29	-	-
	(ii)	51	51	-	-
	(iii)	63	73	-	-

Note that the (i), (ii), and (iii) represent the MRAC-SC, the NAMR-SC, and the conventional PI-SC, respectively.

### C. Comparative Experimental Results between Proposed MRAC-SC, NAMR-SC, and Conventional PI-SC

Fig. 9(a)-(c) demonstrate the comparative experimental results of the proposed MRAC-SC, the NAMR-SC and the conventional PI-SC for Case 1 under parameter variations, respectively. It is clearly shown in Fig. 9(a) that the measured speed ( $\omega$ ) accurately follows the desired speed ( $\omega_d$ ) in the steady-state, and then the rotor speed rapidly tracks  $\omega_d$  with a short settling time (46 ms) and no overshoot in the transient-state. Meanwhile, Fig. 9(b) exhibits the experimental results of the NAMR-SC. In this figure, the speed response shows a longer settling time (62 ms) and no overshoot, also. Moreover, Fig. 9(c) shows the slowest settling time (71 ms) and no overshoot under the same condition of Case 1. Thus, it can be seen that the proposed MRAC-SC has much better performance than the NAMR-SC and the conventional PI-SC in the speed transient behavior because the transient tracking error is speedily compensated.

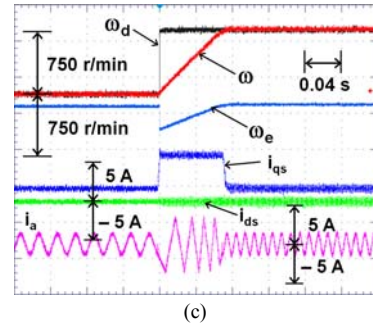


Fig. 9. Experimental results for Case 1 under parameter variations (i.e., +50% variations of  $J$ , +100% variations of  $B$ , -25% variations of  $\phi_r$ , and +20% variations of  $L_s$ ): measured speed ( $\omega$ ), desired speed ( $\omega_d$ ), speed error ( $\omega_e$ ),  $q$ - $d$  axis currents ( $i_{qs}$  and  $i_{ds}$ ), and phase a current ( $i_a$ ). (a) The proposed MRAC-SC. (b) The NAMR-SC. (c) The conventional PI-SC.

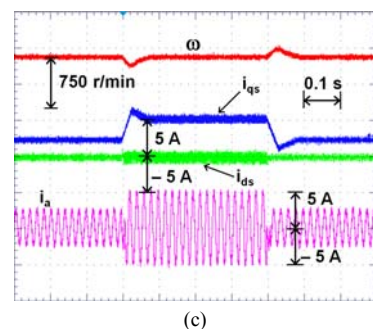
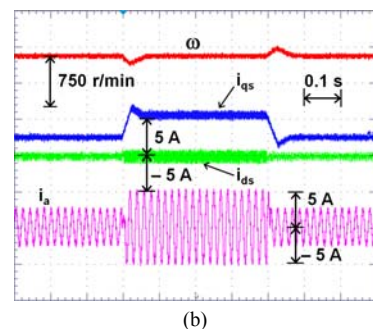
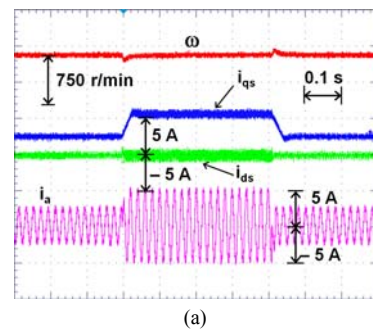


Fig. 10. Experimental results for Case 2 under parameter variations (i.e., +50% variations of  $J$ , +100% variations of  $B$ , -25% variations of  $\phi_r$ , and +20% variations of  $L_s$ ): measured speed ( $\omega$ ),  $q$ - $d$  axis currents ( $i_{qs}$  and  $i_{ds}$ ), and phase a current ( $i_a$ ). (a) The proposed MRAC-SC. (b) The NAMR-SC. (c) The conventional PI-SC.

Next, Fig. 10(a)-(c) display the comparative experimental results of the proposed MRAC-SC, the NAMR-SC, and the conventional PI-SC for Case 2 under parameter variations, respectively. In these figures, it can be clearly observed that the proposed MRAC-SC reveals a shorter settling time (42

ms) and a smaller overshoot (7.3%) than the NAMR-SC (i.e., settling time: 63 ms and speed overshoot: 15.5%) during the transient-time. Meanwhile, the conventional PI-SC depicts the settling time of 70 ms and speed overshoot of 20.8%. Hence, the proposed MRAC-SC can remarkably eliminate the sudden external disturbances thanks to a good adaptation capability.

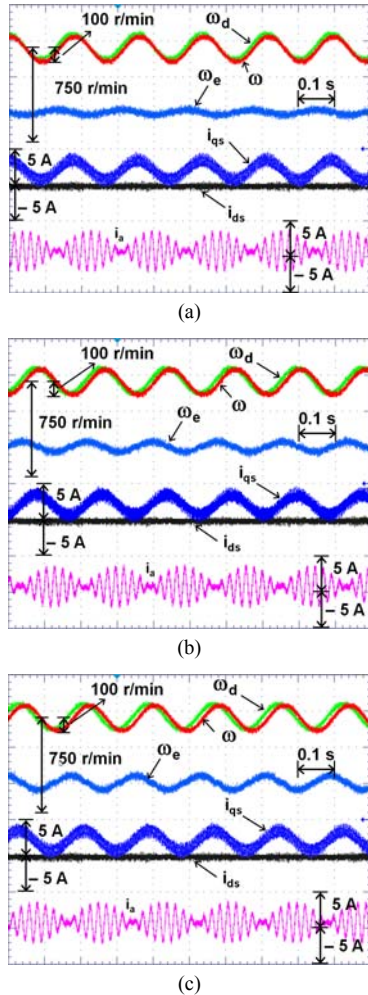


Fig. 11. Experimental results for Case 3 under nominal parameters: measured speed ( $\omega$ ), desired speed ( $\omega_d$ ), speed error ( $\omega_e$ ),  $q$ - $d$  axis currents ( $i_{qs}$  and  $i_{ds}$ ), and phase  $a$  current ( $i_a$ ). (a) The proposed MRAC-SC. (b) The NAMR-SC. (c) The conventional PI-SC.

Fig. 11(a)-(c) show the comparative experimental results of the proposed MRAC-SC, the NAMR-SC, and the conventional PI-SC for a sinusoidal speed reference of  $750 + 100\sin(10\pi t)$  r/min (i.e., Case 3) under nominal parameters, respectively. As observed from Fig. 11(a), the maximum speed error of the proposed MRAC-SC (15 r/min) is much smaller than those of the NAMR-SC (32 r/min) exhibited in Fig. 11(b) and the conventional PI-SC (42 r/min) presented in Fig. 11(c).

Fig. 12(a)-(c) show the comparative experimental results of the proposed MRAC-SC, the NAMR-SC, and the conventional PI-SC for a sinusoidal speed reference of  $750 + 100\sin(10\pi t)$  r/min (i.e., Case 3) under parameter variations, respectively. As observed from Fig. 12(a), the maximum speed error of the proposed MRAC-SC (16 r/min) is much

smaller than those of the NAMR-SC (38 r/min) exhibited in Fig. 12(b) and the conventional PI-SC (45 r/min) presented in Fig. 12(c). It is observed from Figs. 11 and 12 that the NAMR-SC has a smaller error compared to the conventional PI-SC due to the non-adaptive compensating terms. Meanwhile, under this case, the proposed MRAC-SC clearly indicates the excellent sinusoidal speed tracking performance due to its self-adaptation capacity. Based on Figs. 9–12, Table IV summarizes the control performance comparisons of three control schemes (i.e., the proposed MRAC-SC, the NAMR-SC, and the conventional PI-SC) during the transient-state through the experimental results.

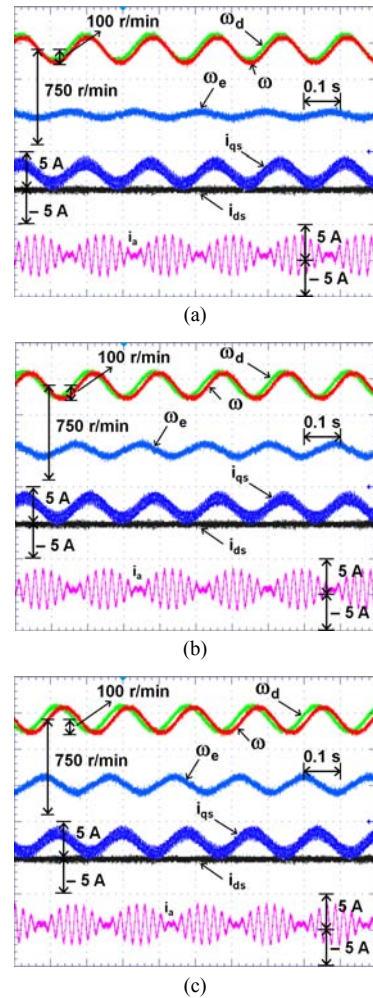


Fig. 12. Experimental results for Case 3 under parameter variations (i.e., +50% variations of  $J$ , +100% variations of  $B$ , -25% variations of  $\varphi_b$ , and +20% variations of  $L_s$ ): measured speed ( $\omega$ ), desired speed ( $\omega_d$ ), speed error ( $\omega_e$ ),  $q$ - $d$  axis currents ( $i_{qs}$  and  $i_{ds}$ ), and phase  $a$  current ( $i_a$ ). (a) The proposed MRAC-SC. (b) The NAMR-SC. (c) The conventional PI-SC.

By analyzing the simulation and experimental results shown in Figs. 5–12, it is worth concluding that the SPMSM drive system using the proposed MRAC-SC can significantly improve the sinusoidal speed tracking response as well as the speed step tracking response.

TABLE IV

CONTROL PERFORMANCE COMPARISONS OF THREE CONTROL SCHEMES DURING THE TRANSIENT TIME VIA EXPERIMENTAL RESULTS

(i) / (ii) / (iii)		Case 1 under parameter variations	Case 2 under parameter variations	Case 3 under nominal parameter	Case 3 under parameter variations
Maximum Speed Error (r/min)	(i)	-	55	15	16
	(ii)	-	116	32	38
	(iii)	-	156	42	45
Overshoot (%)	(i)	0	7.3	-	-
	(ii)	0	15.5	-	-
	(iii)	0	20.8	-	-
Settling Time (ms)	(i)	46	42	-	-
	(ii)	62	63	-	-
	(iii)	71	70	-	-

Note that the (i), (ii), and (iii) represent the MRAC-SC, the NAMR-SC, and the conventional PI-SC, respectively.

### V. CONCLUSION

This paper presents a simple MRAC-based speed control scheme for a SPMSM drive. The main contribution of this scheme is that the speed error converges to zero along with a regulated exponential decay trajectory generated from the reference model. Also, the proposed scheme possesses a disturbance rejection capability because of not requiring any accurate parameters and load torque values of the motor. Mathematically, the asymptotic stability of the proposed MRAC-SC is proven by the Lyapunov stability theory. The validity of the proposed MRAC-based method is illustrated via the simulation and experimental results. Consequently, the SPMSM drive system using the proposed MRAC-SC can achieve a faster dynamic response, a better tracking possibility, and more robustness than the drives using the NAMR-SC and the conventional PI-SC under external disturbances and parameter uncertainties.

### REFERENCES

[1] M. Melfi, S. Evon, and R. McElveen, "Induction versus permanent magnet motors," *IEEE Ind. Appl. Mag.*, vol. 15, no. 6, pp. 28–35, Nov. 2009.

[2] I. Boldea, "Control issues in adjustable-speed drives," *IEEE Ind. Electron. Mag.*, vol. 2, no. 3, pp. 32–50, Sep. 2008.

[3] F. Mwasilu, H. T. Nguyen, H. H. Choi, and J. W. Jung, "Finite set model predictive control of interior PM synchronous motor drives with an external disturbance rejection technique," *IEEE/ASME Trans. Mechatronics*, vol. 22, no. 2, pp. 762–773, Apr. 2017.

[4] M. Paolo, T. Luca, and Z. Mauro, "Torque-ripple reduction in PM synchronous motor drives using repetitive current control," *IEEE Trans. Power Electron.*, vol. 20, no. 6, pp. 1423–1431, Nov. 2005.

[5] M. Tursini, F. Parasiliti, and D. Zhang, "Real-time gain tuning of PI controllers for high-performance PMSM drives," *IEEE Trans. Ind. Appl.*, vol. 38, no. 4, pp. 1018–1026, Jul./Aug. 2002.

[6] G. Zhang and J. Furusho, "Speed control of two-inertia system by PI/PID control," *IEEE Trans. Ind. Electron.*, vol. 47, no. 3, pp. 603–609, Jun. 2000.

[7] R. Errouissi, M. Ouhrouche, W. H. Chen, and A. M. Trzynadlowski, "Robust cascaded nonlinear predictive control of a permanent magnet synchronous motor with antiwindup compensator," *IEEE Trans. Ind. Electron.*, vol. 59, no. 8, pp. 3078–3088, Aug. 2012.

[8] T. D. Do, H. H. Choi, and J. W. Jung, " $\theta$ -D approximation technique for nonlinear optimal speed control design of surface-mounted PMSM drives," *IEEE/ASME Trans. Mechatronics*, vol. 20, no. 4, pp. 1822–1831, Aug. 2015.

[9] J. Yang, W. H. Chen, S. Li, L. Guo, and Y. Yan, "Disturbance/uncertainty estimation and attenuation techniques in PMSM drives—A survey," *IEEE Trans. Ind. Electron.*, vol. 64, no. 4, pp. 3273–3285, Apr. 2017.

[10] J. R. Dominguez, A. Navarrete, M. A. Meza, A. G. Loukianov, and J. Canedo, "Digital sliding-mode sensorless control for surface-mounted PMSM," *IEEE Trans. Ind. Informat.*, vol. 10, no. 1, pp. 137–151, Feb. 2014.

[11] X. Zhang, L. Sun, K. Zhao, and L. Sun, "Nonlinear speed control for PMSM system using sliding-mode control and disturbance compensation techniques," *IEEE Trans. Power Electron.*, vol. 28, no. 3, pp. 1358–1365, Mar. 2013.

[12] S. Li and H. Gu, "Fuzzy adaptive internal model control schemes for PMSM speed-regulation system," *IEEE Trans. Ind. Informat.*, vol. 8, no. 4, pp. 767–779, Feb. 2013.

[13] S. Barkat, A. Tlemcani, and H. Nouri, "Noninteracting adaptive control of PMSM using interval type-2 fuzzy logic systems," *IEEE Trans. Fuzzy Syst.*, vol. 19, no. 5, pp. 925–936, Oct. 2011.

[14] F. F. M. El-Sousy, "Hybrid  $H_\infty$ -based wavelet-neural network tracking control for permanent-magnet synchronous motor servo drives," *IEEE Trans. Ind. Electron.*, vol. 57, no. 9, pp. 3157–3166, Sep. 2010.

[15] F. F. M. El-Sousy, "Intelligent optimal recurrent wavelet Elman neural network control system for permanent-magnet synchronous motor servo drive," *IEEE Trans. Ind. Informat.*, vol. 9, no. 4, pp. 1986–2003, Apr. 2013.

[16] J. W. Jung, V. Leu, T. Do, E. K. Kim, and H. Choi, "Adaptive PID speed control design for permanent magnet synchronous motor drives," *IEEE Trans. Ind. Electron.*, vol. 30, no. 2, pp. 900–908, Feb. 2015.

[17] Y. S. Kung and M. H. Tsai, "FPGA-based speed control IC for PMSM drive with adaptive fuzzy control," *IEEE Trans. Power Electron.*, vol. 22, no. 6, pp. 2476–2486, Nov. 2007.

[18] H. Chaoui and P. Sicard, "Adaptive fuzzy logic control of permanent magnet synchronous machines with nonlinear friction," *IEEE Trans. Ind. Electron.*, vol. 59, no. 2, pp. 1123–1133, Feb. 2012.

[19] H. H. Choi, V. Q. Leu, Y. S. Choi, and J. W. Jung, "Adaptive speed controller design for a permanent magnet synchronous motor," *IET Electr. Power Appl.*, vol. 5, no. 5, pp. 457–464, May 2011.

[20] S. K. Kim, K. G. Lee, and K. B. Lee, "Singularity-free adaptive speed tracking control for uncertain permanent magnet synchronous motor," *IEEE Trans. Power Electron.*, vol. 31, no. 2, pp. 1692–1701, Feb. 2016.

[21] I. D. Landau, "A survey of model reference adaptive techniques—Theory and applications," *Automatica*, vol. 10, pp. 353–379, 1974.

[22] K. J. Astrom and B. Wittenmark, *Adaptive Control*, Addison Wesley, 1995.

[23] T. Orłowska-Kowalska and K. Szabat, "Control of the drive system with stiff and elastic couplings using adaptive neuro-fuzzy approach," *IEEE Trans. Ind. Electron.*, vol. 54, no. 1, pp. 228–240, Feb. 2007.

[24] H. Z. Jin and J. M. Lee, "An RMRAC current regulator for permanent magnet synchronous motor based on statistical model interpretation," *IEEE Trans. Ind. Electron.*, vol. 56, no. 1, pp. 169–177, Jan. 2009.

[25] L. Guo and L. Parsa, "Model reference adaptive control of five-phase IPM motors based on neural network," *IEEE Trans. Ind. Electron.*, vol. 59, no. 3, pp. 1500–1508, Mar. 2012.

[26] A. V. R. Teja, C. Chakraborty, S. Maiti, and Y. Hori, "A new model reference adaptive controller for four quadrant vector controlled induction motor drives," *IEEE Trans. Ind. Electron.*, vol. 59, no. 10, pp. 3757–3767, Oct. 2012.

[27] K. J. Astrom and T. Hagglund, *Advanced PID control*, ISA-Instrumentation, Systems, and Automation Society, 2005.

[28] K. J. Astrom and B. Wittenmark, *Computer-Controlled Systems—Theory and Design*. Englewood Cliffs, NJ: Prentice-Hall, 1990.

[29] W. Liang, J. Wang, P. C. K. Luk, W. Fang, and W. Fei, "Analytical modeling of current harmonic components in PMSM drive with voltage-source inverter by SVPWM technique," *IEEE Trans. Energy Convers.*, vol. 29, no. 3, pp. 673–680, Sep. 2014.

[30] M. L. Corradini, G. Ippoliti, S. Longhi, and G. Orlando, "A quasi-sliding mode approach for robust control and speed estimation of PM synchronous motors," *IEEE Trans. Ind. Electron.*, vol. 59, no. 2, pp. 1096–1104, Feb. 2012.

[31] J. X. Xu, S. K. Panda, Y. J. Pan, T. H. Lee, and B. H. Lam, "A modular control scheme for PMSM speed control with pulsating torque minimization," *IEEE Trans. Ind. Electron.*, vol. 51, no. 3, pp. 526–536, Jun. 2004.

[32] Y. A. R. I. Mohamed, "Design and implementation of a robust current-control scheme for a PMSM vector drive with a simple adaptive

disturbance observer.” *IEEE Trans. Ind. Electron.*, vol. 54, no. 4, pp. 1981-1988, Aug. 2007.

- [33] X. Li and S. Li, “Speed control for a PMSM servo system using model reference adaptive control and an extended state observer,” *Journal of Power Electronics*, vol. 14, no. 3, pp. 549-563, May 2014.



**Anh Tuan Nguyen** received the B.S. and M.S. degrees in electrical engineering from Hanoi University of Science and Technology, Hanoi, Vietnam, and the M.S. degree in electrical engineering from Grenoble Institute of Technology, Joseph Fourier University, Grenoble, France, in 2010, 2012, and 2015, respectively. He is currently working toward the Ph.D. degree in the Division of Electronics and Electrical Engineering, Dongguk University, Seoul, Korea.

His current research interests include electric power system, control of power converters, and DSP-based electric machine drives.



**Muhammad Saad Razaq** received the B.S. degree in electrical engineering from the University of Engineering and Technology, Taxila, Pakistan, in 2011, and is currently working toward the Ph.D. degree in the Division of Electronics and Electrical Engineering, Dongguk University, Seoul, Korea.

From 2012 to 2013, he was a Laboratory Engineer in the University of Gujrat, Gujrat, Pakistan. His current research interests include distributed generation systems, electric vehicles, and DSP-based electric machine drives.



**Han Ho Choi** (M'03) received the B.S. degree in control and instrumentation engineering from Seoul National University (SNU), Seoul, Korea, and the M.S. and Ph.D. degrees in electrical engineering from the Korea Advanced Institute of Science and Technology (KAIST), Daejeon, Korea, in 1988, 1990, and 1994, respectively.

He is currently in the Division of Electronics and Electrical Engineering, Dongguk University, Seoul, Korea. His research interests include control theory and its application to real-world problems.



**Jin-Woo Jung** (M'06) received the B.S. and M.S. degrees in electrical engineering from Hanyang University, Seoul, Korea, and the Ph.D. degree in electrical and computer engineering from The Ohio State University, Columbus, OH, USA, in 1991, 1997, and 2005, respectively.

From 1997 to 2000, he was in the Home Appliance Research Laboratory, LG Electronics Co., Ltd., Seoul, Korea. From 2005 to 2008, he was a Senior Engineer in the R&D Center and in the PDP Development Team, Samsung SDI Co., Ltd., Korea. Since 2008, he has been a Professor in the Division of Electronics and Electrical Engineering, Dongguk University, Seoul, Korea. His research interests include DSP-based electric machine drives, distributed generation systems using renewable energy sources, and power conversion systems and drives for electric vehicles.